Journal of Electron Spectroscopy and Related Phenomena 184 (2011) 29–37

Contents lists available at ScienceDirect

Journal of Electron Spectroscopy and Related Phenomena

journal homepage: www.elsevier.com/locate/elspec

# X-ray photoelectron spectroscopy studies of reactions on chromium metal and chromium oxide surfaces

B.P. Payne[a,*], M.C. Biesinger[b], N.S. McIntyre[a]

[a] Department of Chemistry, The University of Western Ontario, London, ON N6A 5B7, Canada
[b] Surface Science Western, The University of Western Ontario, London, ON N6A 5B7, Canada

ARTICLE INFO

*Article history:*
Received 17 August 2010
Received in revised form 1 December 2010
Accepted 2 December 2010
Available online 8 December 2010

*Keywords:*
$Cr_2O_3$
$Cr(OH)_3$
XPS
Cr oxidation

ABSTRACT

This paper reports several interrelated XPS investigations of the Cr–O system that provide additional interpretation of the Cr $2p_{3/2}$ spectra, along with more detail on the reaction mechanisms between $O_2$ gas and $H_2O$ vapour with metallic Cr. The Cr $2p_{3/2}$ spectra of polycrystalline $Cr_2O_3$ contain multiplet structures that bear a strong resemblance to those calculated by Gupta and Sen for the free $Cr^{3+}$ ion. The O/Cr ratio derived from the corrected $Cr^{3+}$ and substitutional $O^{2-}$ intensities for all polycrystalline $Cr_2O_3$ samples was 1.5. Annealing of freshly cleaved polycrystalline $Cr_2O_3$ surfaces above 550 °C resulted in a sharpening of the multiplet structures that may be caused by the increased prevalence of the (0 0 0 1) $Cr_2O_3$ orientation on the surface. The slight difference in binding energies between the low energy (0 0 0 1) plane and the other major crystallographic orientations could contribute to the spectral broadening that is observed for the Cr $2p_{3/2}$ spectral line shapes. The Cr $2p_{3/2}$ spectrum for $Cr(OH)_3$ was isolated from that produced by $Cr_2O_3$ and the multiplet structure was qualitatively re-assembled for that of the hydroxide. The Cr $2p_{3/2}$ and O 1s spectra of reaction products on polycrystalline metal surfaces were analysed using the above information. The oxidic portion of the Cr $2p_{3/2}$ spectra could be cleanly separated from the metallic substrate using spectral subtraction. Reactions of either $O_2$ gas or $H_2O$ vapour both produced a thin $Cr_2O_3$ film that was deficient in $Cr^{3+}$ and, depending on the reactant, showed varying concentrations of hypo-stoichiometric Cr moieties. The surface corrected O/Cr ratios calculated for all the oxidised surfaces were 1.7. There was little evidence to support the formation of $Cr(OH)_3$ on these surfaces. For comparison, an aqueous reaction of a Ni–Cr (20%) alloy was studied where both $Cr(OH)_3$ and $Cr_2O_3$ components could be analysed. For this example no sub-stoichiometric Cr oxide species were produced.



## 1. Introduction

An understanding of the reactions that occur on Cr surfaces is important as the element is added to many materials to increase their corrosion resistance. At temperatures below 400 °C thin $Cr_2O_3$ film growth on metallic Cr has been shown to follow a Cabrera–Mott model [1–6], where oxidation is driven by an electric field created by electrons tunnelling through the oxide film from the Cr metal substrate. Cations and/or anions are mobile in this electric field and move through defect sites and grain boundaries, resulting in the formation of thin oxide films [1–5]. It has been shown that $Cr_2O_3$ is primarily a p-type oxide where cations are most mobile, however some anion migration has also been identified [1–6].

This paper presents an XPS study of Cr metal surfaces following reactions with $O_2$ gas, $H_2O$ vapour, and in an aqueous solution. This work was done to provide a more complete base for the subsequent study of surfaces of a Ni–Cr (20%) alloy subjected to aqueous corrosion at controlled electrochemical potentials and temperatures. XPS is useful for such studies as it provides both compositional and chemical state information over an information depth of ~5 nm – a thickness encompassing both the metal substrate and the surface oxides. The XPS spectra of Cr oxides are rich in additional structure from multiplet splitting; previous papers have provided significant details on these spectral structures [7–11], but additional information regarding both $Cr_2O_3$ and $Cr(OH)_3$ spectral features and elemental intensity ratios have been obtained in this work. Using this information, surfaces of polycrystalline Cr metal following gas phase reactions with $O_2$ or $H_2O$ at 300 °C could be shown to contain a sub-stoichiometric $Cr_2O_3$ ($Cr_{2+\delta}O_{3-\delta}$) component. By contrast, during aqueous oxidation of

* Corresponding author. Tel.: +1 519 661 2111x86703.
*E-mail address:* bpayne2@uwo.ca (B.P. Payne).

0368-2048/$ – see front matter © 2010 Elsevier B.V. All rights reserved.
doi:10.1016/j.elspec.2010.12.001

**Table 1**
The XPS surface composition in at.%.

| Sample/Treatment | Composition (at.%) | | | |
|---|---|---|---|---|
| | Cr | O | C | Other |
| $Cr_2O_3$-1 (powder pressed into a polyethylene tape) | 23.3 | 47.9 | 28.8 | |
| $Cr_2O_3$-2 (powder pressed into a polyethylene tape) | 22.4 | 48.2 | 28.6 | Na 0.8 |
| $Cr_2O_3$-3 (fractured aggregate, heated 550 °C, 3 h) | 22.4 | 45.0 | 22.5 | Ca 0.6, Cl 0.5, Mg 1.1, Na 5.3, Si 2.7 |
| $Cr_2O_3$-4 (fractured aggregate, heated 550 °C, 3 h) | 22.9 | 46.8 | 19.8 | Ca 1.4, Cl 0.6, Mg 0.7, Na 4.8, Si 3.0 |
| $Cr(OH)_3 \cdot xH_2O$ (powder pressed into a polyethylene tape) | 6.4 | 29.4 | 63.7 | Ca 0.5 |
| Cr metal (polished, $Ar^+$ sputtered, 15 min, annealed, 600 °C, 30 min) | 92.1 | 3.7 | 1.9 | Ar 2.3 |
| Cr metal-1 + $O_2$, 300 °C, 1 Torr, $6.0 \times 10^7$ L | 34.6 | 43.0 | 20.7 | Ar 1.3, N 0.3 |
| Cr metal-2 + $O_2$, 300 °C, 1 Torr, $2.4 \times 10^8$ L | 32.6 | 46.3 | 20.0 | Ar 1.1 |
| Cr metal-3 + $H_2O$, 300 °C, 1 Torr, $3.0 \times 10^7$ L | 42.9 | 29.1 | 26.5 | Ar 1.5 |
| Cr metal-4 + $H_2O$, 300 °C,1 Torr, $3.0 \times 10^7$ L | 46.5 | 29.9 | 22.2 | Ar 1.5 |
| NiCr metal + pH 5, 0.001 M $(NH_4)_2SO_4$, 150 °C, 72 h | 4.4 | 45.4 | 33.2 | Cl 1.5, Ni 12.3, N 0.7, S 2.6 |

a Ni–Cr (20%) alloy, only $Cr_2O_3$ and $Cr(OH)_3$ contributions were detected.

## 2. Experimental

All XPS analysis was carried out using a Kratos Axis Ultra spectrometer employing a monochromatic Al Kα (15 mA, 14 kV) X-ray source. The work function and the dispersion of the instrument were calibrated to give metallic Au $4f_{7/2}$ and Cu $2p_{3/2}$ signals of 83.95 eV and 932.63 eV respectively. All XPS analysis employed the hybrid-focusing lens, a scan time of 180 s, and an analysis area of 700 μm × 300 μm. Differential surface charging on insulating samples was minimised using the Kratos charge neutraliser system with a filament current between 1.7–1.8 A and a charge balance of 2.8 V. Survey spectra were collected at a pass energy of 160 eV with a 0.7 eV energy step over a binding energy (BE) range of 1100–0 eV. Analyses of the Cr 2p, O 1s and C 1s envelopes were carried out at a pass energy of 20 eV, an energy step size of 0.05 eV, over energy ranges of 595–565 eV (30–70 sweeps), 540–520 eV (5–15 sweeps), and 295–275 eV (10–20 sweeps) respectively. Pressures near $5 \times 10^{-9}$ Torr were observed in the analytical chamber during surface analysis.

A polycrystalline $Cr_2O_3$ powder was obtained from Sigma Aldrich having 99.9% purity. Polycrystalline $Cr_2O_3$ aggregates (~2–3 mm in size) and polycrystalline Cr metal pieces (1–25 mm in size) were obtained from Alfa Aesar having purity levels of 99.6% and 99.9% respectively. A Ni–Cr (20%) rod was obtained from ACI Alloys Incorporated. Samples of a $Cr_2O_3$ powder were pressed into a double-sided, non-conducting polyethylene polymer prior to XPS analysis to minimise the chance of differential surface charging. The $Cr_2O_3$ aggregates were fractured under vacuum in a chamber having a base pressure of $1 \times 10^{-8}$ Torr and then heated in the same chamber for 3 h (plus 30 min ramp time) at 550 °C. Samples of Cr metal were prepared for gas phase oxidation by polishing to a mirror finish using 0.05 μm γ-$Al_2O_3$ paste followed by sonication in methanol for 20 min. Following sonication, the specimens were introduced to the XPS system ($1 \times 10^{-8}$ Torr) for surface cleaning. Surfaces were sputtered for 15 min using a 4 kV $Ar^+$ ion beam having an emission current of 15 mA followed by annealing at 600 °C for 30 min. The respective amounts of O and C present following ion etching were found to be less than 5 atomic % (at.%) by XPS. This amount of contamination could not be removed with additional sputtering/annealing cycles.

In situ oxidation of Cr metal samples was carried out in an adjacent chamber having a base pressure of $7 \times 10^{-7}$ Torr. Metallic surfaces were exposed to high purity $O_2$ (99.99%) gas for doses of $6.0 \times 10^7$ and $2.4 \times 10^8$ Langmuir (L) at 300 °C and 1 Torr. Additional samples were exposed to $H_2O$ vapour for doses of $3.0 \times 10^8$ L at 300 °C and 1 Torr. Similar experiments studying the reactivity of Fe and Ni with both $O_2$ gas and $H_2O$ vapour have been completed in this chamber [12–15].

A metal disk (~3 mm thick) was cut from the polycrystalline Ni–Cr (20%) rod and prepared by polishing to a mirror finish using 0.05 μm γ-$Al_2O_3$ paste followed by sonication in methanol for 20 min. The sample was oxidised electrochemically at 150 °C in an autoclave for 72 h in 0.001 M $(NH_4)_2SO_4$ adjusted to a pH of 5 with $H_2SO_4$. The potential was held constant at 0 V versus a 0.1 M saturated Ag/AgCl reference electrode.

All XPS spectra were analysed using CasaXPS Version 2.3.14 [16]. The background for all spectra was subtracted using a Shirley baseline [16]. The at.% of each element present was determined from XPS survey spectra (see Table 1). The total amount of Cr present on each surface was calculated using the area of the Cr $2p_{3/2}$ peak only. In each case the relative sensitivity factor (RSF) [16] for the Cr 2p envelope (2.427) was adjusted to a value of 1.618 as the $2p_{3/2}$ region contains 2/3 of the total area of the Cr 2p peak. The same correction factor was previously employed by this group to study the oxidation of polycrystalline Ni metal surfaces with $H_2O$ vapour [15]. This area correction was applied because a definitive end to the M $2p_{3/2}$ (M = Cr or Ni) region was not evident from sample to sample, while a very distinct separation between the $2p_{3/2}$ and $2p_{1/2}$ peaks was observed on all survey spectra. The RSF values for the O 1s and C 1s spectra were 0.780 and 0.278 respectively. Fitting of the high-resolution spectra was completed using components having mixed Gaussian–Lorentzian character. The Cr $2p_{3/2}$ envelopes were best fit using Gaussian (40%)–Lorentzian (60%) line shapes, which are denoted as GL(60) in CasaXPS. The O 1s and C 1s regions were best fit with components having GL(50) and GL(30) profiles respectively. To compare the different Cr, O, and C species present the total atomic concentrations (see Table 1) were corrected using the peak area ratios obtained from the fitting of the respective high-resolution spectra (see Tables 2–4).

All specimens studied as a part of this work were found to contain significant amounts of adventitious C (see Table 1). A representative C 1s spectrum collected from the $Cr_2O_3$-2 powder sample is shown in Fig. 1. All C 1s spectra were dominated by a strong hydrocarbon (C–C, C–H) signal, which was used for spectral calibration of insulating samples and corrected to a BE of 284.8 ± 0.1 eV. Additional spectral intensity assigned to alcohol/ether (–COH, –COC–, O=C(O–C*)), carbonyl (–C=O), and ester (O=CO–) functionalities were also observed at respective BEs of 286.2 ± 0.1 eV, 287.7 ± 0.1 eV, and 288.6 ± 0.2 eV [17]. A small peak was found at 289.6 ± 0.2 eV on all of the oxidised metallic Cr samples and attributed to a carbonate ($-CO_3^{2-}$) species. A previous publication by this group had assigned the peak at 286.2 ± 0.1 eV solely to a –COH group [15]. For the above peak assignments to be valid a minimum area ratio of 1:1 was required between the components centered at 286.2 ± 0.1 eV and 288.6 ± 0.2 eV. In cases where the intensity of the lower BE peak was found to be greater

**Table 2**
Summary of the organic C 1s peak areas and calculated contributions to the corresponding O 1s spectra.

| Sample | Total C 1s (at.%) | Contributions from C to the C 1s spectra | | | | | | | | | Total O 1s (at.%) | Calculated contributions from O to the O 1s spectra | | | | | | | |
|---|---|---|---|---|---|---|---|---|---|---|---|---|---|---|---|---|---|---|---|
| | | –COH/–COC/O═C(O–C*) | | | –C═O | | O═CO– | | $-CO_3^{2-}$ | | | O═CO– | | –C═O | | –COH/–COC– | | $-CO_3^{2-}$ | |
| | | C 1s (%) | [a]at.% | [b]at.% | C 1s (%) | at.% | C 1s (%) | at.% | C 1s (%) | at.% | | [c]at.% | O 1s (%) | at.% | O 1s (%) | [d]at.% | O 1s (%) | at.% | O 1s (%) |
| $Cr_2O_3$-1 | 28.8 | 19.2 | 0.9 | 4.6 | 0.8 | 0.2 | 3.1 | 0.9 | | | 47.9 | 1.8 | 3.8 | 0.2 | 0.4 | 3.1 | 6.5 | | |
| $Cr_2O_3$-2 | 28.6 | 12.6 | 1.2 | 2.4 | 1.4 | 0.4 | 4.2 | 1.2 | | | 48.2 | 2.4 | 5.0 | 0.4 | 0.8 | 1.6 | 3.3 | | |
| $Cr_2O_3$-3 | 22.5 | 3.2 | 0.5 | 0.2 | 1.8 | 0.4 | 2.1 | 0.5 | | | 45.0 | 1.0 | 2.2 | 0.4 | 0.9 | 0.1 | 0.2 | | |
| $Cr_2O_3$-4 | 19.8 | 2.5 | 0.2 | 0.3 | 1.3 | 0.3 | 1.2 | 0.2 | | | 46.8 | 0.4 | 0.9 | 0.3 | 0.6 | 0.2 | 0.4 | | |
| $Cr(OH)_3{\cdot}xH_2O$ | 63.7 | 7.9 | 3.5 | 1.5 | 0.2 | 0.1 | 5.5 | 3.5 | | | 29.4 | 7.0 | 23.8 | 0.1 | 0.3 | 1.0 | 3.4 | | |
| Cr metal-1 | 20.7 | 5.1 | 1.1 | | 8.1 | 1.7 | 5.1 | 1.1 | 2.5 | 0.5 | 43.0 | 2.2 | 5.1 | 1.7 | 4.0 | | | 1.5 | 3.5 |
| Cr metal-2 | 20.0 | 6.3 | 1.3 | | 9.1 | 1.8 | 6.3 | 1.3 | 3.7 | 0.7 | 46.3 | 2.6 | 5.6 | 1.8 | 3.9 | | | 2.1 | 4.5 |
| Cr metal-3 | 26.5 | 5.1 | 1.4 | | 2.5 | 0.7 | 5.1 | 1.4 | 0.8 | 0.2 | 29.1 | 2.8 | 9.6 | 0.7 | 2.4 | | | 0.6 | 2.1 |
| Cr metal-4 | 22.2 | 6.0 | 1.3 | | 4.1 | 0.9 | 6.0 | 1.3 | 1.5 | 0.3 | 29.9 | 2.6 | 8.7 | 0.9 | 3.0 | | | 0.9 | 3.0 |
| NiCr metal | 33.2 | 6.1 | 0.3 | 1.7 | 0.8 | 0.3 | 0.9 | 0.3 | | | 45.4 | 0.6 | 1.3 | 0.3 | 0.7 | 1.1 | 2.4 | | |

* Carbon atom giving rise to the C 1s signal.
[a] Normalised surface C concentration for the O═C(O–C*) group.
[b] Combined normalised surface C concentration for the assumed 1:1 mixture of –COH/–COC– species.
[c] The normalised surface O concentration could be calculated using either the O═C(O–C*) or O═CO– values from the C 1s analyses.
[d] The normalised surface O concentration for the assumed 1:1 mixture of –COH/–COC– species was estimated using an O/C ratio of 2:3.

**Table 3**
Cr $2p_{3/2}$ peak fits for the polycrystalline $Cr_2O_3$, $Cr(OH)_3$, and Cr metal samples.

| Sample | FWHM (eV) | Peak 1 (eV) | Area (%) | Peak 2 (eV) | Area (%) | Peak 3 (eV) | Area (%) | Peak 4 (eV) | Area (%) | Peak 5 (eV) | Area (%) |
|---|---|---|---|---|---|---|---|---|---|---|---|
| $Cr_2O_3$-1 | 1.05 | 575.4 | 34.2 | 576.4 | 29.4 | 577.1 | 22.1 | 578.0 | 9.1 | 578.8 | 5.2 |
| $Cr_2O_3$-2 | 1.03 | 575.7 | 34.7 | 576.7 | 30.2 | 577.3 | 21.2 | 578.2 | 8.7 | 579.0 | 5.2 |
| $Cr_2O_3$-3[a] | 0.96 | 575.6 | 34.1 | 576.6 | 30.3 | 577.3 | 19.8 | 578.2 | 8.5 | 579.0 | 5.1 |
| $Cr_2O_3$-4[a] | 0.99 | 575.8 | 34.9 | 576.8 | 30.2 | 577.5 | 19.7 | 578.4 | 8.6 | 579.2 | 4.7 |
| $Cr(OH)_3{\cdot}xH_2O$ oxide component[b] | 1.03 | 575.7 | 4.7 | 576.7 | 4.1 | 577.4 | 2.9 | 578.2 | 1.2 | 579.0 | 0.8 |
| hydroxide component | 1.32 | 576.3 | 28.1 | 577.1 | 23.3 | 577.8 | 21.9 | 578.5 | 9.3 | 579.5 | 3.8 |
| Cr metal[c] | | 574.1 | 75.2 | 574.8 | 20.3 | 576.8 | 4.5 | | | | |

[a] Additional peaks at $574.0 \pm 0.1$ eV were also required to completely fit the Cr $2p_{3/2}$ spectra for the fractured and heated aggregates.
[b] The $Cr_2O_3$ contribution was estimated using the fit obtained for the $Cr_2O_3$-2 powder sample.
[c] The Cr metal Cr $2p_{3/2}$ spectrum was fit with 3 peaks which do not represent Cr species in different chemical environments. The envelope was fit with an asymmetric component having the line shape LA(1.3,2.3,10) and a FWHM of 0.77 eV, while peaks 2 and 3 had a line shape of GL(30) and FWHM values of 2.16 eV.

**Table 4**
O 1s peak fits for the $Cr_2O_3$, $Cr(OH)_3$, oxidised Cr, and oxidised NiCr metal samples.

| Sample | Peak 1 (eV) | Area (%) | FWHM (eV) | Peak 2 (eV) | Area (%) | FWHM (eV) | Peak 3 (eV) | Area (%) | FWHM (eV) | Organics (%) |
|---|---|---|---|---|---|---|---|---|---|---|
| $Cr_2O_3$-1 | 530.0 | 70.7 | 1.07 | 531.2 | 24.5 | 1.92 | 532.9 | 4.8 | 1.39 | 10.7 |
| $Cr_2O_3$-2 | 530.3 | 69.7 | 1.04 | 531.6 | 27.6 | 2.01 | 533.2 | 2.7 | 1.40 | 9.1 |
| $Cr_2O_3$-3 | 530.2 | 81.7 | 1.03 | 531.4 | 18.3 | 2.09 | | | | 3.3 |
| $Cr_2O_3$-4 | 530.4 | 79.2 | 1.03 | 531.6 | 20.8 | 2.24 | | | | 1.9 |
| $Cr(OH)_3 \cdot xH_2O$ | 529.7 | 4.5 | 1.02 | 531.6 | 87.5 | 1.81 | 533.5 | 8.0 | 1.25 | 27.5 |
| [a] $OH^-$ only | | | | | 60.0 | | | | | |
| Cr metal–1 | 530.2 | 72.4 | 1.37 | 531.9 | 27.6 | 1.57 | | | | 12.6 |
| Cr metal–2 | 530.2 | 74.2 | 1.41 | 531.8 | 25.8 | 1.53 | | | | 14.0 |
| Cr metal–3 | 530.0 | 64.2 | 1.29 | 531.5 | 35.8 | 1.81 | | | | 14.1 |
| Cr metal–4 | 530.0 | 61.2 | 1.32 | 531.5 | 38.8 | 1.81 | | | | 14.7 |
| NiCr metal | 529.6 | 1.5 | 1.35 | 531.7 | 97.0 | 1.65 | 533.6 | 1.4 | 1.45 | 4.4 |

[a] Peak area calculated by subtracting the total organic contribution from the $OH^-$ component.

than the peak at 288.6 ± 0.2 eV the additional spectral intensity was assumed to be split equally between C atoms bound as –COH and –COC–. The organic contribution to the O 1s spectra was estimated by first calculating the surface normalised C intensities. From these intensities the corresponding normalised O concentrations were obtained using the expected O/C ratios for the individual functional groups (i.e. 1:1 for –C=O). The normalised O concentrations were then converted to the respective O 1s peak areas. This procedure is summarised in Table 2.

The CasaXPS program was also used for spectral subtractions. To simplify the analysis of the oxidised metal surfaces, the metal contribution was removed. A similar technique was previously employed by this group to study the oxidation of Ni metal [14,15,18].

## 3. Results and discussion

### 3.1. Spectral refinements for $Cr_2O_3$

Two samples of a polycrystalline $Cr_2O_3$ powder were analysed with XPS and a representative high-resolution Cr $2p_{3/2}$ spectrum is shown in Fig. 2(a). The spectra collected from both samples were fit with 5 peaks representing the multiplet splitting of the $Cr^{3+}$ cations following photoionization (see Table 3). The fits produced using this approach agree well with the $2p_{3/2}$ line shape calculated for a $Cr^{3+}$ free ion by Gupta and Sen [7,8,11]. Two polycrystalline $Cr_2O_3$ aggregates were fractured and heated (550 °C) *in vacuo* and the freshly fractured surfaces were analysed by XPS. The Cr $2p_{3/2}$ fitting results were found to be very similar to those for the polycrystalline $Cr_2O_3$ powder (see Table 3). Heating of the aggregates resulted in a narrowing of the 5 multiplet splitting components relative to what was observed for the polycrystalline $Cr_2O_3$ powder samples (see Table 3). As well, a small component near 574 eV [11] was also required to fit the envelope. A fitted representative Cr $2p_{3/2}$ spectrum is shown in Fig. 3(a). The observed difference in peak widths is attributed to the formation of an oxide surface that is primarily oriented in the (0 0 0 1) direction following heating at 550 °C. Previous LEED studies have shown that annealing of polycrystalline $Cr_2O_3$ surfaces near this temperature lead to a crystal reorganisation to form the low surface energy (0 0 0 1) plane [19,20].

The O 1s spectra collected for all polycrystalline $Cr_2O_3$ samples were fit with an $O^{2-}$ component at 530.2 ± 0.2 eV, along with additional broad peaks at BEs ranging from 531.2 to 533.2 eV (see Table 4). Example spectra are presented in Figs. 2 and 3(b). As was shown in a previous publication, some of the intensity of the high BE peaks can be attributed to the presence of organic species associated with adventitious C [15]. The contribution of these organic

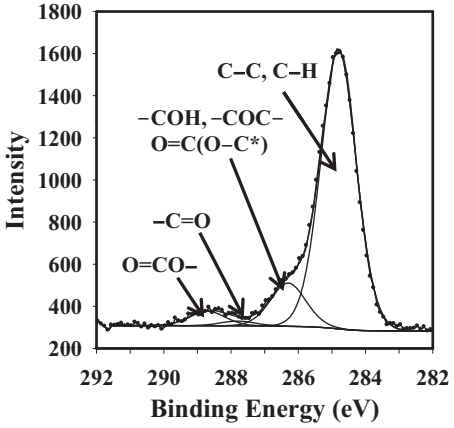


**Fig. 1.** A representative high-resolution C 1s spectrum collected from a sample of polycrystalline $Cr_2O_3$ powder.

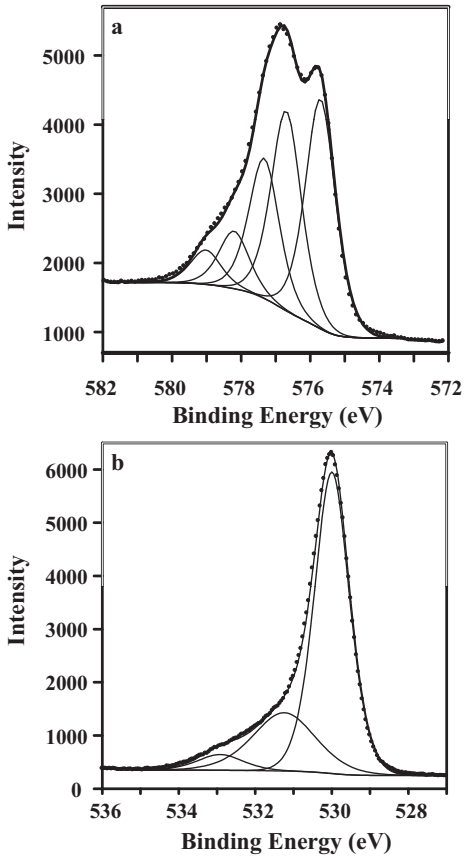


**Fig. 2.** The high-resolution (a) Cr $2p_{3/2}$ and (b) O 1s spectra for a polycrystalline $Cr_2O_3$ powder.

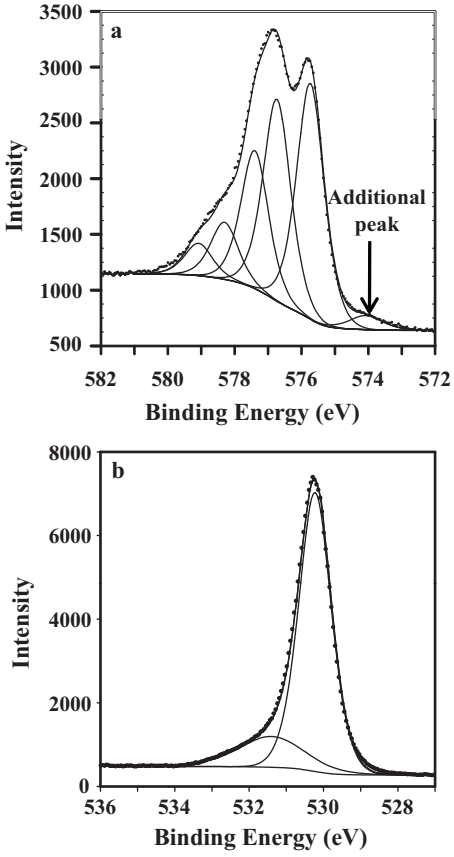


**Fig. 3.** The high-resolution (a) Cr $2p_{3/2}$ and (b) O 1s spectra of a vacuum fractured $Cr_2O_3$ aggregate following annealing at 550 °C for 3 h.

species to the O 1s spectra have been estimated, and the results are presented in Table 4. Additional contributions from adsorbed O and/or OH surface species cannot be ruled out. Small amounts of Ca, Mg, Na, and Si (see Table 1) were also detected on the aggregate samples during compositional analysis and some of the intensity in the O 1s peaks may arise from the presence of the oxides and/or hydroxides of these species. The O/Cr ratios for the polycrystalline powder samples were calculated using the normalised surface intensities of the $O^{2-}$ and $Cr^{3+}$ components and were determined to be 1.5 (see Table 5). This result indicates that the presence of significant amounts of surface $Cr(OH)_3$ is unlikely as the calculated O/Cr ratios are identical to the expected value of 1.5 for pure $Cr_2O_3$. A similar method was used to determine the O/Ni ratios in a previous publication [15]. A slight increase in the O/Cr ratio was observed on the heated polycrystalline aggregate samples (see

**Table 5**
O/Cr ratios calculated from the normalised surface concentrations.

| | Normalised surface concentration (at.%) | | | |
|---|---|---|---|---|
| Sample | $O^{2-}$ or $OH^-$ | Cr metal | Oxidized Cr | O/Cr |
| $Cr_2O_3$-1 | 33.9 | | 23.3 | 1.5 |
| $Cr_2O_3$-2 | 33.6 | | 22.4 | 1.5 |
| $Cr_2O_3$-3 | 36.8 | | 22.4 | 1.6 |
| $Cr_2O_3$-4 | 37.1 | | 22.9 | 1.6 |
| $Cr(OH)_3{\cdot}xH_2O$ oxide | 1.3 | | 0.9 | 1.5 |
| [a]Hydroxide | 17.6 | | 5.5 | 3.2 |
| Cr metal-1 | 31.1 | 16.4 | 18.2 | 1.7 |
| Cr metal-2 | 34.4 | 12.3 | 20.3 | 1.7 |
| Cr metal-3 | 18.7 | 31.9 | 11.0 | 1.7 |
| Cr metal-4 | 18.3 | 35.8 | 10.7 | 1.7 |

[a] The hydroxide surface concentration was calculated using the organic subtracted $OH^-$ peak area from Table 4.

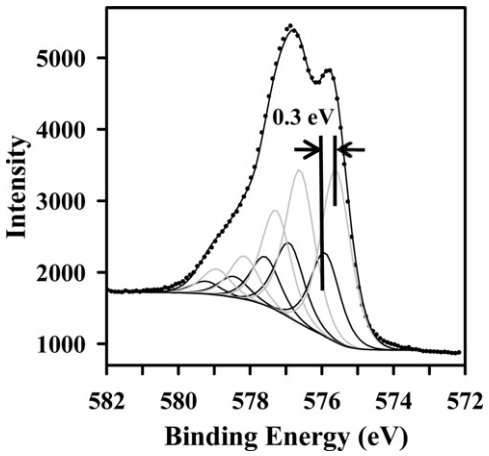


**Fig. 4.** The high-resolution Cr $2p_{3/2}$ spectrum of a polycrystalline $Cr_2O_3$ powder fit with two sets of overlapping multiplet splitting peaks representing $Cr^{3+}$ atoms in the (0 0 0 1) plane (black lines) and all other crystallographic orientations (grey lines).

Table 5) relative to pure $Cr_2O_3$. This result may be attributed to the presence of Ca, Mg, and Na oxide impurities, which have $O^{2-}$ BE shifts similar to that of $Cr_2O_3$ [21–23]. As with the $Cr_2O_3$ powder samples, this result suggests that little $Cr(OH)_3$ is present on the aggregate surfaces.

The Cr $2p_{3/2}$ spectra collected from the polycrystalline powder samples were re-fit using two overlapping sets of the 5 multiplet splitting peaks obtained from the analysis of sample $Cr_2O_3$-3 (see Table 3). A representative Cr $2p_{3/2}$ spectrum is shown in Fig. 4, in which the centroids of the 5 peaks for the two $Cr_2O_3$ components are offset by 0.3 eV. Analysis of the Cr $2p_{3/2}$ spectrum of the second polycrystalline powder sample yielded a separation of 0.4 eV between the centroids of the two overlapping components. This small observed shift is attributed to the differences in BE between the $Cr^{3+}$ atoms orientated in the (0 0 0 1) plane (black lines) and those in the other major crystallographic orientations (grey lines) [24]. The spectrum for a polycrystalline powder would be expected to be somewhat broadened by the presence of the oxide in orientations each with its own particular BE; and this could be one of several reasons for the broadening observed in the 2p spectra of many metal oxides. Although spectral broadening due to differential surface charging cannot be completely ruled out, any charging effects are thought to be small due to the use of a charge neutraliser during XPS analysis and the fact that the samples were pressed into a non-conducting polyethylene tape. Thus, this work has served to better define the Cr $2p_{3/2}$ and O 1s line shapes and positions for differing orientations of $Cr_2O_3$, as well as show that an O/Cr ratio for the appropriate peaks mirrors that for the known stoichiometry.

### 3.2. Spectral refinements for $Cr(OH)_3$

The XPS spectra collected from a hydrated $Cr(OH)_3{\cdot}xH_2O$ powder presented in an earlier publication (see Fig. 4 in Ref. [11]) has been re-analysed here. In the original analysis it was determined that a small $Cr_2O_3$ impurity was present [11]. Refitting of the O 1s spectrum (see Fig. 5(a)) showed a small $O^{2-}$ component at 529.7 eV, a large peak representing the overlapping signal from substitutional $OH^-$ and adsorbed organic species at 531.6 eV, and a third peak attributed to $H_2O$ of hydration at 533.5 eV (see Table 4). From the O 1s analysis it was determined that 4.5% of the total O present was in the $O^{2-}$ state (see Table 4). Using the O/Cr ratio for $Cr_2O_3$ (1.5), the corresponding $Cr^{3+}$ contribution to the Cr $2p_{3/2}$ spectrum was estimated to be 13.7% and was modeled using the fits obtained from analysis of the polycrystalline powder sample $Cr_2O_3$-2 (see Table 3). After constraining the area of the $Cr_2O_3$ component to

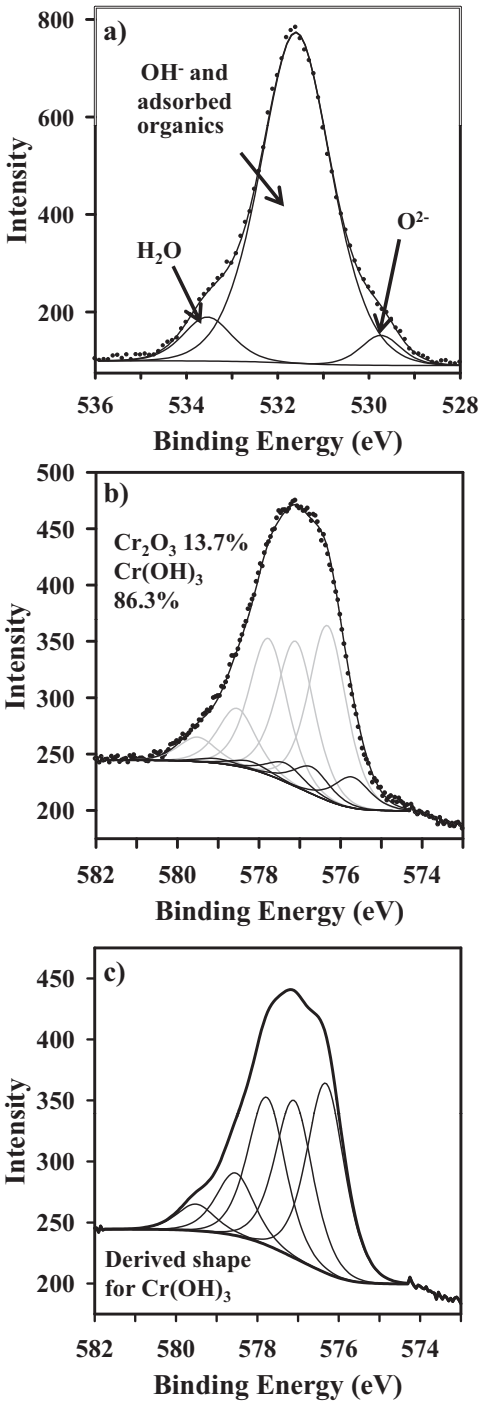


**Fig. 5.** The high-resolution (a) O 1s and (b) Cr $2p_{3/2}$ spectrum for $Cr(OH)_3{\cdot}xH_2O$. The Cr $2p_{3/2}$ spectrum was fit with contributions from both $Cr_2O_3$ (black lines) and $Cr(OH)_3$ (grey lines). The high-resolution spectrum for pure $Cr(OH)_3$ reconstructed using the combined intensities of the obtained 5 multiplet splitting peaks is shown in (c). The original Cr $2p_{3/2}$ spectrum was presented previously by Biesinger et al. [11].

account for 13.7% of the total Cr $2p_{3/2}$ spectrum, the remaining intensity representing pure $Cr(OH)_3$ was fit with 5 multiplet splitting peaks having identical FWHM values (see Table 3). Fig. 5(b) shows the Cr $2p_{3/2}$ spectrum fit with both $Cr_2O_3$ (black lines) and $Cr(OH)_3$ (grey lines) components. The resultant pure spectrum for $Cr(OH)_3$ is presented in Fig. 5(c). An O/Cr ratio of 3.2 was obtained when the surface normalised substitutional $OH^-$ component from the O 1s spectrum was compared to the surface corrected $Cr(OH)_3$ contribution determined from the fitting of the Cr $2p_{3/2}$ spectrum. This result is close to the expected value of 3 for pure $Cr(OH)_3$ and suggests that the hydroxide and oxide components have been cleanly separated using this method. It is important to note that the total $OH^-$ surface concentration was determined by subtracting the contribution from the adsorbed organic species from the total area of the peak located at 531.6 eV in the O 1s spectrum (see Table 4).

### 3.3. Reactions of metallic Cr with $O_2$ and $H_2O$

Clean polycrystalline Cr metal surfaces were exposed to ultra pure $O_2$ gas for doses of $6.0 \times 10^7$ and $2.4 \times 10^8$ L at 300 °C and a pressure of 1 Torr. Two additional metal samples were exposed to a $3.0 \times 10^8$ L dose of $H_2O$ vapour under the same temperature and pressure conditions. Representative Cr $2p_{3/2}$ spectra produced by reactions with $O_2$ gas for a dose of $2.4 \times 10^8$ L and $H_2O$ vapour for a dose of $3.0 \times 10^8$ L are shown in Fig. 6(a) and (b). A strong metal signal at $573.6 \pm 0.1$ eV was observed on all surfaces indicating the formation of thin oxide films. Fitting of the Cr $2p_{3/2}$ spectra shown in Fig. 6(a) and (b) was undertaken to separate the metallic contributions from those of the oxide. The metal portion of each spectrum was fit using the metal components presented in Table 3. The remaining spectral intensity was then assigned to the oxidic component. The corresponding O 1s spectra (see Fig. 6(c) and (d)) were fit with an $O^{2-}$ component at $530.1 \pm 0.1$ eV and a peak attributed to adsorbed surface species at $531.7 \pm 0.2$ eV (see Table 2). The O/Cr ratios were calculated using the corrected $O^{2-}$ and non-metallic Cr surface intensities and found to be 1.7 for all samples (see Table 5). This result suggests that these films are deficient in $Cr^{3+}$ and is supported by the low temperature oxidation mechanism first presented by Cabrera and Mott for p-type transition metal oxides [1–5]. In the case of Cr metal, the oxidation reaction involves the formation of $Cr^{3+}$ vacancies at the oxide/gas interface. Over time there is an inward migration of these vacancies towards the metal substrate in an electric field set up by electrons tunnelling through the oxide film. At the same time metallic Cr atoms are oxidised at the metal/oxide interface and travel through these vacancy sites as well as grain boundaries to the oxide/gas interface, where they react with either $O_2$ or $H_2O$ promoting further film growth [1–5].

To better observe the structure of the oxidised Cr species, the metal peak was removed and the resultant subtracted spectra are shown in Fig. 6(e) and (f). After spectral subtraction the oxide components were cleanly separated. These spectra were then fit with the line shape obtained previously for the polycrystalline $Cr_2O_3$ powder ($Cr_2O_3$-2 from Table 3). Most of the envelope was well fit with the line shape for $Cr_2O_3$, however additional contributions to the reaction spectra were clearly detected at the low BE side of the $Cr_2O_3$ envelopes. We attribute this to a hypo-stoichiometric $Cr_2O_3$ ($Cr_{2+\delta}O_{3-\delta}$) component that is likely formed during the initial stages of the reaction. To our knowledge this species has not been observed previously using XPS; its presence is somewhat comparable to the formation of $Ni^{3+}$ during initial oxidation of Ni metal [14,15]. The exact nature of this Cr species is not identified here as there was no model structure available. However, in a previous study on the oxidation of Cr metal, it was suggested that film growth proceeded through the formation of $Cr^{3+}$ and $O^{2-}$ vacancies [6,25]. Both of these vacancies are said to carry a negative charge and to maintain charge balance, $Cr^{2+}$ cations are created and are situated in the interstitial sites of the $Cr_2O_3$ film [6,25]. The subtracted Cr $2p_{3/2}$ spectra collected from the $H_2O$ dosed surfaces showed the largest contributions from the hypo-stoichiometric component relative to the regular $Cr_2O_3$. This is probably the result of the thin nature of these films, as the sub-stoichiometric component would comprise a larger portion of the oxide. However, it is also possible that incorporation of other species such as H, a product of the dissocia-

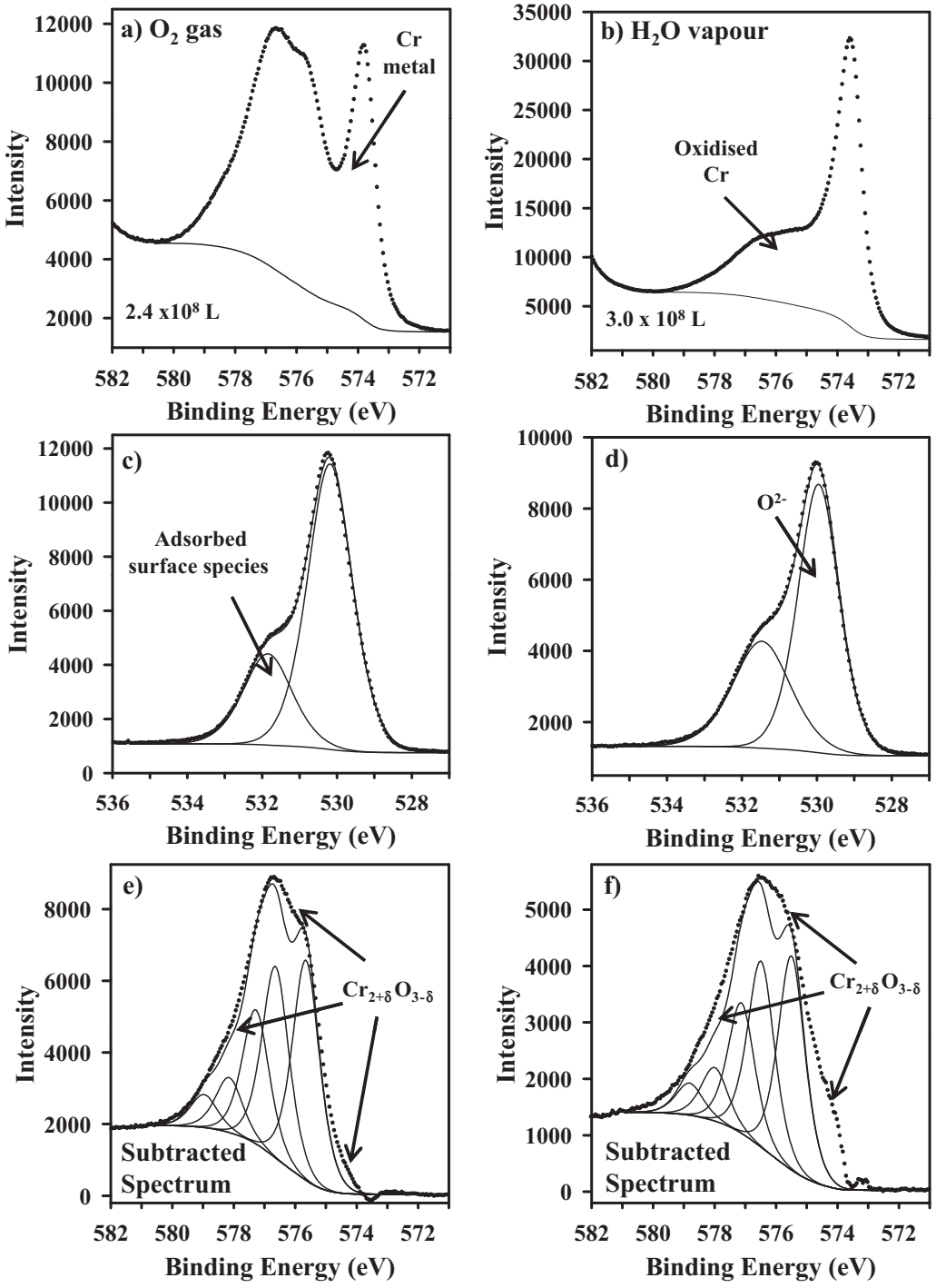


**Fig. 6.** The high-resolution Cr $2p_{3/2}$ spectra collected from metal surfaces following doses of (a) $2.4 \times 10^8$ L of $O_2$ gas and (b) $3.0 \times 10^8$ L of $H_2O$ vapour at 300 °C and 1 Torr. The O 1s spectra for the (c) $2.4 \times 10^8$ L of $O_2$ gas and (d) $3.0 \times 10^8$ L of $H_2O$ vapour are also shown. The metal component was removed from each Cr $2p_{3/2}$ spectrum and the resultant subtracted spectra for doses of (e) $2.4 \times 10^8$ L of $O_2$ gas and (f) $3.0 \times 10^8$ L dose of $H_2O$ vapour are also presented. The subtracted spectra show the possible presence of a hypo-stoichiometric $Cr_2O_3$ oxide.

tion of $H_2O$, into some of the $Cr^{3+}$ vacancies may lead to increased formation of this hypo-stoichiometric film. The presence of H in cation vacancy sites has previously been suggested to retard film growth on both Ni and Fe metal surfaces following reaction with $H_2O$ vapour [13,15,26]. Some contributions are also observed in the subtracted spectra around 580 eV that may be attributed to the formation of Cr cations in higher oxidation states. It is unlikely that the peak broadening observed in the subtracted spectra (Fig. 6(e) and (f)) is due to differential charging, given the proximity of the metal substrate.

The high BE peak found near $531.7 \pm 0.2$ eV in the O 1s spectra has a similar chemical shift to that of $OH^-$ (see Table 4) however, the presence of significant levels of $Cr(OH)_3$ on any of the oxidised surfaces is unlikely on the basis of the observed O/Cr ratios. From the analysis of the accompanying C 1s spectra it was determined that a significant amount of the intensity of the high BE O 1s peak results from the presence of adsorbed organic species (see Tables 2 and 4). It is believed that the remaining intensity would result from the presence of adsorbed O and/or OH species, which are possible intermediates in the oxidation reaction [5].

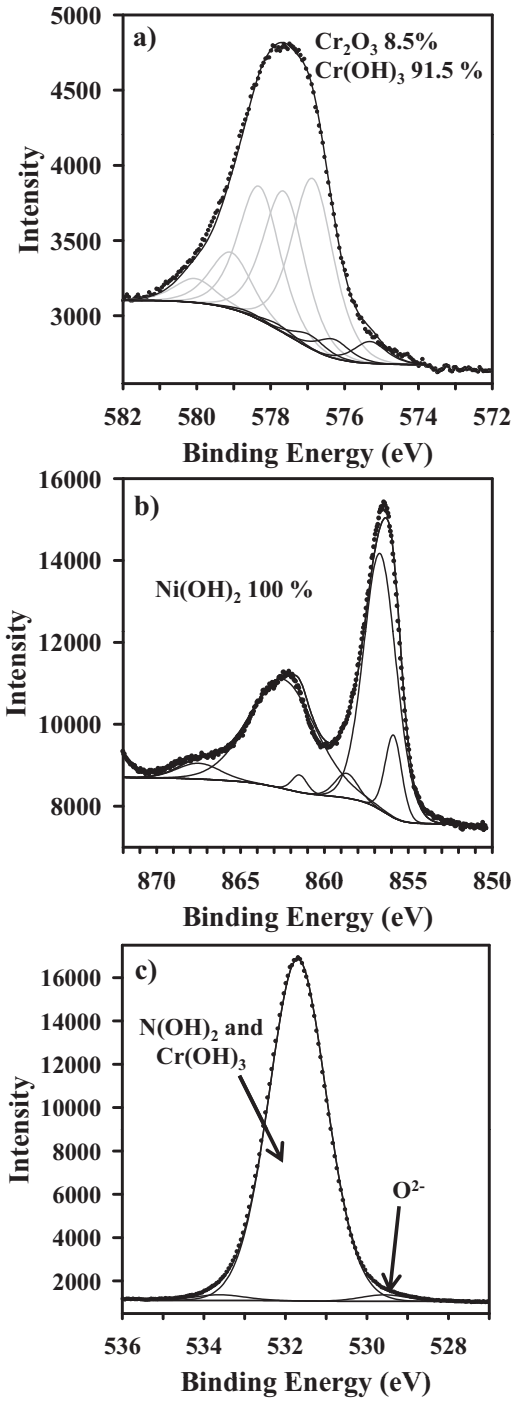


**Fig. 7.** The high-resolution (a) Cr $2p_{3/2}$ spectrum from a Ni–Cr (20%) alloy surface containing a mixture of $Cr_2O_3$ (black lines) and $Cr(OH)_3$ (grey lines). The corresponding (b) Ni $2p_{3/2}$ and (c) O 1s spectra are also shown.

### 3.4. Aqueous reaction of metallic Ni–Cr (20%)

Fig. 7(a) contains the Cr $2p_{3/2}$ high-resolution spectra collected from a Ni–Cr (20%) alloy electrochemically oxidised at 150 °C for a 72 h period at a pH of 5. The spectrum was fit with contributions from the polycrystalline $Cr_2O_3$ (black lines, $Cr_2O_3$-2) and $Cr(OH)_3$ (grey lines) powders presented in Table 3, and a good fit of the envelope was observed. A small $O^{2-}$ peak in the O 1s spectrum at 529.6 eV was observed and verified the presence of $Cr_2O_3$ (see Fig. 7(c)). None of the $O^{2-}$ signal could be attributed to NiO, as the analysis of the Ni $2p_{3/2}$ spectrum (see Fig. 7(b)) showed all oxidised Ni species were present as $Ni(OH)_2$. The Ni $2p_{3/2}$ spectrum was fit using the components for $Ni(OH)_2$ presented in a previous publication [18]. There was no spectral evidence to suggest that a sub-stoichiometric Cr species formed under these oxidation conditions.

## 4. Conclusions

The Cr $2p_{3/2}$ spectra collected from samples of polycrystalline $Cr_2O_3$ powder were found to exhibit a multiplet structure very similar to that predicted by Gupta and Sen for the free $Cr^{3+}$ ion. The narrowest Cr $2p_{3/2}$ spectra were obtained following annealing of fractured surfaces to 550 °C. Heating of the samples is believed to result in conversion of polycrystalline surface structures to a single (0 0 0 1) orientation having a slightly different BE than that for the polycrystalline surface. A small separation in BE was observed between the $Cr^{3+}$ atoms oriented in the (0 0 0 1) direction relative to those found in the other major crystallographic arrangements. Additionally, a possible line shape for the Cr $2p_{3/2}$ spectrum for $Cr(OH)_3$ was modeled using synthetic components from a sample containing contributions from both $Cr_2O_3$ and $Cr(OH)_3$.

Analysis of the Cr $2p_{3/2}$ spectra collected from metallic Cr surfaces exposed to both $O_2$ gas and $H_2O$ vapour showed the formation of thin $Cr^{3+}$ deficient $Cr_2O_3$ films with a contribution from a hypo-stoichiometric component ($Cr_{2+\delta}O_{3-\delta}$). The concentration of this Cr species was found to be greater on the surfaces exposed to $H_2O$ vapour. No $Cr(OH)_3$ appears to form following exposure to $H_2O$ vapour. A different result was observed following the aqueous oxidation of a Ni–Cr (20%) alloy, with contributions from both $Cr_2O_3$ and $Cr(OH)_3$ observed in the Cr $2p_{3/2}$ spectrum. There was no spectral evidence to suggest the formation of a hypo-stoichiometric Cr species.

## Acknowledgements

Dr. Jamie Noël and Dr. Pellumb Jakupi are thanked for their help in performing the high temperature electrochemical oxidation experiment. An additional thanks is extended to Dr. David Shoesmith for the use of his laboratory and equipment. The financial assistance of the Natural Research Council of Canada (NSERC) is also acknowledged.

## References

[1] G.A. Hope, I.M. Ritchie, J. Chem. Soc., Faraday Trans. 1 77 (1981) 2621.
[2] F.P. Fehlner, N.J. Graham (Eds.), Corrosion Mechanisms in Theory and Practice, Marcel Decker Inc., New York, 1995 (Chapter 4).
[3] D.J. Young, M. Cohen, J. Electrochem. Soc.: Solid-State Sci. Technol. 124 (1977) 769.
[4] J.S. Arlow, D.F. Michell, M.J. Graham, J. Vac. Sci. Technol. A 5 (4) (1987) 572.
[5] N. Cabrera, N.F. Mott, Rep. Prog. Phys. 12 (1948–1949) 163.
[6] K. Hauffe, Oxidation of Metals, Plenum Press, New York, 1965 (Chapter 4).
[7] R.P. Gupta, S.K. Sen, Phys. Rev. B 10 (1) (1974) 71.
[8] R.P. Gupta, S.K. Sen, Phys. Rev. B 12 (1) (1975) 15.
[9] A.R. Pratt, N.S. McIntyre, Surf. Interface Anal. 24 (1996) 529.
[10] N.S. McIntyre, A.R. Pratt, H. Piao, D. Maybury, S.J. Splinter, Appl. Surf. Sci. 144–145 (1999) 156.
[11] M.C. Biesinger, C. Brown, J.R. Mycroft, R.D. Davidson, N.S. McIntyre, Surf. Interface Anal. 36 (2004) 1550.
[12] A.P. Grosvenor, B.A. Kobe, N.S. McIntyre, Surf. Sci. 565 (2004) 151.
[13] A.P. Grosvenor, B.A. Kobe, N.S. McIntyre, Surf. Sci. 572 (2005) 217.
[14] B.P. Payne, A.P. Grosvenor, M.C. Biesinger, B.A. Kobe, N.S. McIntyre, Surf. Interface Anal. 39 (2007) 582.
[15] B.P. Payne, M.C. Biesinger, N.S. McIntyre, J. Electron. Spectrosc. 175 (2009) 55.
[16] N. Fairley, CasaXPS Version 2.2.107, 1999–2005.
[17] G. Beamson, D. Briggs, High-resolution XPS of Organic Polymers the Scienta ESCA300 Database, John Wiley and Sons, Toronto, 1992 (Appendices 1–3).
[18] M.C. Biesinger, B.P. Payne, L.W.M. Lau, A. Gerson, R.St.C. Smart, Surf. Interface Anal. 41 (2009) 324.

[19] V. Maurice, S. Cadot, P. Marcus, Surf. Sci. 458 (2000) 195.
[20] C.P. Huggins, R.M. Nix, Surf. Sci. 594 (2005) 163.
[21] H. Van Doveren, J.A.Th. Verhoeven, J. Electron Spectrosc. Relat. Phenom. 21 (1980) 265.
[22] V.I. Nefedov, M.N. Firsov, I.S. Shaplygin, J. Electron Spectrosc. Relat. Phenom. 26 (1982) 65.
[23] A. Barrie, F.J. Street, J. Electron Spectrosc. Relat. Phenom. 7 (1977) 1.
[24] S.P. McBride, A.J. Bell, in: ISAF 2002: Proceedings of the 13th IEEE International Symposium on Applications of Ferroelectrics, 2002, p. 451.
[25] K. Hauffe, J. Block, Z. Physik. Chem. 198 (1951) 232.
[26] A.P. Grosvenor, J.T. Francis, B.A. Kobe, N.S. McIntyre, Surf. Interface Anal. 37 (2005) 495.